A Numerical Model of Radar Scattering from Steep and Breaking Waves

A. G. Voronovich and V. U. Zavorotny
NOAA/Earth System Research Laboratory
325 Broadway
Boulder, CO 80305-3328

Abstract—**Ocean gravity waves can be rather steep and even breaking depending on wind speed. Analytical modeling of both the evolution of such strongly nonlinear waves and electromagnetic (EM) scattering from them is currently impossible. At the same time, numerical modeling of these processes poses a significant challenge in terms of the complexity of codes and computational time. In this study, we employ an efficient and fast numerical solver which is based on a uniform approach equally convenient when dealing with both hydrodynamic and EM parts of the problem. As a result, a sequence of large-scale wave profiles is produced that follows through all stages of wave breaking. The small-scale roughness is treated statistically by employing the Pierson-Moskowitz spectrum, and it is added on top of smooth gravity waves. Using the EM code, the scattering problem is solved assuming an impedance boundary condition. The same spline description of the surface profiles of gravity waves is used in both hydrodynamic and EM codes. Backscattering cross sections and corresponding Doppler spectra were the subjects of this study. The numerical calculations demonstrate spike events, with the backscattered signal at horizontal polarization exceeding the backscattering signal at vertical polarization.**

I. INTRODUCTION

Radar sea spikes with a high horizontal-to-vertical polarization ratio are commonly observed at moderate and low-grazing-angle (LGA) incidence and are usually attributed to scattering from breaking waves [1, 2]. However, analytical models, such as a two-scale model, or numerical models based on the small-slope approximation and similar approaches do not reproduce such features [3]. This is not unusual since those models describe the ocean gravity waves as rather gentle undulations which only moderately affect Bragg radar scattering from small-scale waves. In reality, depending on the wind speed, gravity waves could be rather steep and even breaking. Rigorous analytical modeling of such strongly nonlinear waves and electromagnetic (EM) scattering from them is currently impossible.

Numerical modeling of EM scattering from breaking waves has been considered previously (see, e.g. [4], [5]). In those works, the profiles of breaking waves were taken from the experiment or generated independently. In our work, both hydrodynamic and EM components were calculated using related codes based on the same wave-profile approximations using cubic splines. The solver consists of three blocks. In the first one, the hydrodynamic equations are solved for potential 2-D surface waves (including surface tension but without viscosity). As a result, a sequence of large-scale wave profiles is produced that includes all stages of wave breaking: steepening, cresting, involution, and jetting. The two last stages produce non-single-valued profiles, which is a substantial obstacle for many existing analytical and numerical approaches but poses no difficulty for our approach. The second block deals with 2-D bistatic EM scattering from those profiles, assuming their periodicity and the impedance boundary conditions for two orthogonal polarizations. Finally, in the third block, using surface fields previously obtained as sources, the Bragg scattering cross section from the small-scale waves is calculated and added to the cross sections from breaking waves. Small-scale roughness is treated statistically by employing the Pierson-Moskowitz spectrum with a cutoff wave number three times smaller than that of the EM wave.

II. MODELING OF BREAKING WAVES

The equations describing the evolution of surface gravity-capillary waves in 2-D are taken in the Lagrangian form:

$$\frac{dx(t,s)}{dt} = \frac{\partial \varphi(t,s)}{\partial x}, \quad \frac{dz(t,s)}{dt} = \frac{\partial \varphi(t,s)}{\partial z}, \tag{1}$$

$$\frac{d\varphi(t,s)}{dt} = \frac{1}{2}(\nabla\varphi)^2 - gz + \sigma\left(\frac{\partial x}{\partial s}\frac{\partial^2 z}{\partial s^2} - \frac{\partial z}{\partial s}\frac{\partial^2 x}{\partial s^2}\right). \tag{2}$$

Here, parameter s marks individual fluid particles on the fluid surface; it is assumed to be an arch length. All derivatives of the velocity potential in (1-2) are calculated at the surface points. Equation (1) represents the kinematic boundary condition and (2) is the Bernoulli equation (note the change of sign of term $(\nabla\varphi)^2/2$ due to use of the Lagrangian description.) Thus, the surface profile is given here in the parametric form and it can be non-single-valued in (x, z) Cartesian coordinates.

Potential φ satisfies the Laplace equation. If functions $x(t,s)$, $z(t,s)$, and $\varphi(t,s)$ are known at a certain moment of time, one can solve the Dirichlet boundary problem and calculate the Dirichlet-to-Neumann (DtN) linear operator which maps the value of surface potential $\varphi(t,s)$ onto the

normal derivative of the potential, $\partial\varphi/\partial\vec{n}$, at the surface points. Since potential φ along the surface is known, the DtN operator allows us to calculate the gradient of the potential (i.e., the velocity vector) at the surface points. Those values are substituted into the right-hand side of (1) and (2), and now one can calculate the surface profile and values of the surface potential at the next moment of time. Marching in time in numerical simulations is accomplished according to the Runge-Kutta scheme.

The problem is thus reduced to the calculation of the DtN operator, which should be effective and accurate. Here, the surface profile is assumed to be periodic, and after conformal mapping $x_0 + iz_0 = \exp[i(x+iz)]$, the whole 2-D lower half-space is transformed into an area bounded by a closed contour on the (x', z') plane (the depth of the fluid is supposed to be infinite.) A solution of the Laplace equation is sought in the form of a double potential:

$$\varphi(\vec{r}) = \int \mu(s') \frac{\partial G_0(\vec{r}'-\vec{r})}{\partial\vec{n}} ds' \quad , \tag{3}$$

where $G_0(\vec{r}) = \ln|\vec{r}|$, and s is an arc length; $\mu(s)$ is the surface density of dipoles. Details on a numerical solution of this equation can be found in [6].

The accuracy of the solution including the stage of the incipient overturning of the wave was controlled by the energy conservation relative accuracy, which was held up to $10^{-5} - 10^{-4}$.

The evolution of the profiles that ended in breaking was obtained by using the superposition of two waves as an initial condition. Each of these waves represents an individually stable, moderately nonlinear Stokes wave. However, after the crests of two waves propagating at different speeds overlap, the wave starts to overturn. Immediately after overturning, the wave profile looses smoothness, the spline approximation becomes inadequate, some accuracy control criteria are violated, and the program stops.

The evolution of such a wave over the first 0.54 seconds has been examined and then used for EM scattering simulations. The initial surface wave length was 1 m. Figure 1 illustrates the wave evolution over the first 0.5 seconds. It was observed that at $t = 0.45\ s$, the front face of the wave becomes almost vertical, and then the wave breaks.

III. MODELING OF RADAR SCATTERING

The calculation of scattering of an EM wave from a periodic 2-D surface reduces to the solution of a scalar Helmholtz equation $\left(\partial^2/\partial x^2 + \partial^2/\partial z^2 + K^2\right)\Psi = 0$ with boundary condition
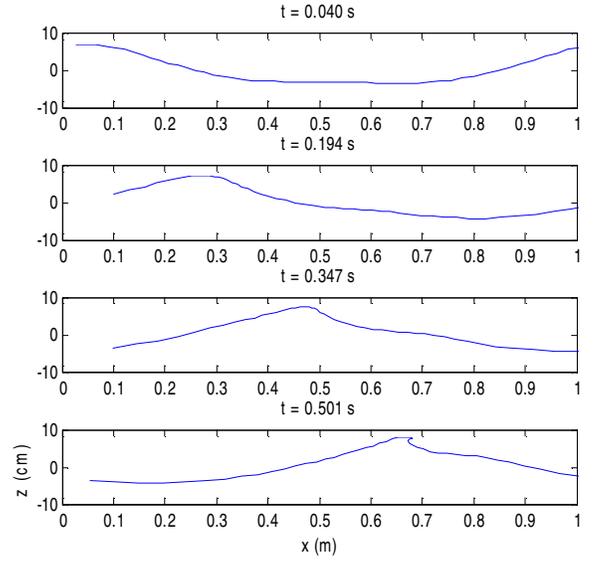
Figure 1. The evolution of a gravity wave.

$$\frac{\partial\Psi}{\partial\vec{n}} = -iKZ\Psi, \quad \vec{r} = (x,z)\in\Sigma. \tag{4}$$

The value of impedance Z depends on the polarization: $Z = 1/\sqrt{\varepsilon+1}$ for vertical, and $Z = \sqrt{\varepsilon-1}$ for horizontal polarization. The problem reduces to the solution of the following integral equation with respect to the surface value of the total field (s) [7]:

$$\frac{1}{2}\Psi(\vec{r}) + \int \Psi(\vec{r}')\left(\frac{\partial}{\partial\vec{n}_{\vec{r}'}} + iKZ\right)\left(-\frac{i}{4}H_0^{(1)}\left(K|\vec{r}-\vec{r}'|\right)\right)d\Sigma_{\vec{r}'} = \Psi_{in}(\vec{r}). \tag{5}$$

Here, $k_0 = K\sin\theta_0$, $q_0 = K\cos\theta_0$ are horizontal and vertical components of the wave vector of the incident wave and

$$G(\vec{r}) = -\frac{i}{4}H_0^{(1)}\left(K|\vec{r}-\vec{r}'|\right) \tag{6}$$

is a Green function. By extracting the phase factor associated with the incident wave from the surface field we introduce a new unknown function [7]:

$$\widetilde{\Psi}(s) = \Psi(s)\exp[-ik_0 x(s) + iq_0 z(s)]. \tag{7}$$

In terms of $\widetilde{\Psi}$, after simple calculations (5) becomes as follows:

$$\widetilde{\Psi}(s) + \frac{1}{2}\int\widetilde{\Psi}(s')\left[iKH_1^{(1)}\left(K|\vec{r}-\vec{r}'|\right)\frac{\frac{dx'}{ds'}(z'-z) - \frac{dz'}{ds'}(x'-x)}{|\vec{r}-\vec{r}'|} + \right.$$
$$\left. + KZH_0^{(1)}\left(K|\vec{r}-\vec{r}'|\right)\right]\exp[k_0(x'-x) - iq_0(z'-z)]ds' = 2. \tag{8}$$

The surface profile $x(s)$, $z(s)$, and surface field $\tilde{\Psi}(s)$ are represented with the help of the same spline approximation as in the hydrodynamic solver. To calculate the interaction matrix, one should be able to calculate the Hankel functions. An effective way to make such a calculation appears to be tabulating of the values of the Hankel functions on a sufficiently dense grid (say, 1000 values) between 0 and 100, and using an asymptotic expansion for larger arguments. Between grid points, they can be calculated using a power expansion whose coefficients immediately follow from the differential equation for Bessel functions.

This allows us to achieve machine accuracy of 10^{-15} rather quickly. When $\vec{r}'$ tends to $\vec{r}$, the Hankel function includes a logarithmic singularity that has to be handled separately. For periodic surfaces, the scattered field consists of discrete spectra:

$$\Psi = \exp(ik_0 x - iq_0 z) + \sum_n S_n \exp(ik_n x - iq_n z), \qquad (9)$$

where $k_n = k_0 + 2\pi n / L$, $q_n = \sqrt{K^2 - k_n^2}$, and L is the period of the surface along the x-axis. The values of spectra can be easily expressed in terms of the surface field.

The contribution from the small-scale roughness can be calculated using the following expression [7]:

$$\sigma_B(k_0) = \frac{1}{L} \int 4K^3 C(s, k_0) \hat{W}_{sw}(s, 2k_s) ds, \qquad (10)$$

where $\hat{W}_{sw}(s, 2k_l)$ is the local spectral density of small-scale roughness, and

$$C(s, k_0) = \frac{1}{16} \left| 1 - Z^2 + i \frac{Z}{KR_0} \right|^2 |\Psi_0|^4 \qquad (11)$$

is a scattering coefficient that accounts for all shadowing effects.

III. DISCUSSION OF RESULTS

Using a sequence of 180 wave profiles obtained for every 0.003 s, the normalized backscattering cross section (NBCS) was calculated based on the numerical technique presented above. For calculations, the EM wavelength = 4.65 cm, and the scattering order $n = -40$ have been chosen, which corresponds to an incident angle of 68.466°. The case considered here was for an "upwind" orientation with respect to the breaking wave, i.e., the incident EM wave vector is pointed toward the face slope of the wave. To model cases of various orthogonal polarizations, two extreme values of complex impedance Z have been chosen. For HH polarization, it is $Z = 0 + i10^3$ and for VV polarization, it is $Z = 0 + i10^{-3}$.

The results of NBCS calculations as a function of time are presented in Figures 2–4. It is seen that generally, the cross section grows with time for all polarizations as the wave becomes steeper.

Figure 2 shows the result of our calculations for normalized backscattering cross section at HH- and VV-polarization at 68.5 degree incidence for strongly nonlinear waves alone. Because wave slopes are gentle enough for the first 0.25 s, the curves represent just the numerical noise. After that, signals start to increase. During the last 0.1 s the signal at VV-polarization is reaching the level of ~ -30 dB, and the signal at HH-polarization is reaching the level of -20 dB, with the HH-polarized signal finally exceeding the level of the VV-polarized signal by about 10 dB.
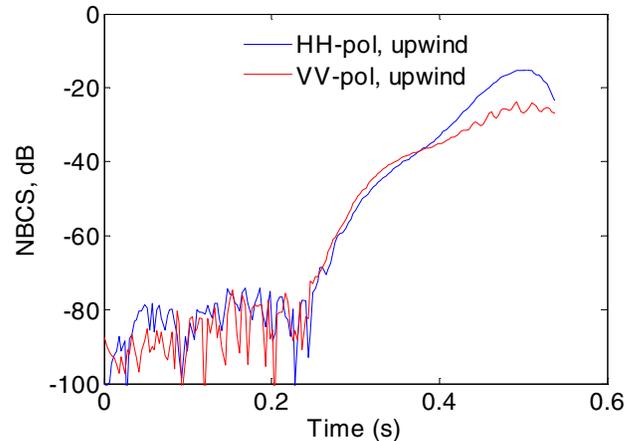
Figure 2. HH- and VV-polarization NBCS at 68.5° incidence for nonlinear waves alone.

Using surface EM fields obtained at the first step of calculation of backscattering from a large-scale nonlinear wave as sources for the small-perturbation theory, Bragg-type scattering on the small-scale roughness is calculated. In Figure 3, the VV-polarization signal of Bragg-scattering origin is compared with the signal from a breaking wave that does not have those Bragg-scattering ripples. One can see that even for the case of a strongly nonlinear breaking wave, Bragg scattering at VV-polarization still exceeds scattering at VV-polarization from a breaking wave.
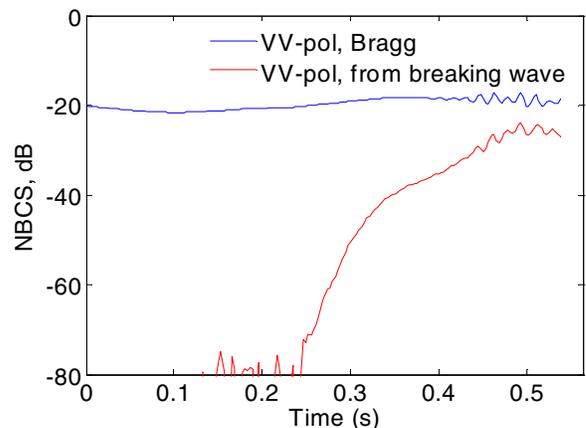
Figure 3. VV-polarization NBCS at 68.5° incidence a nonlinear breaking wave and for small-scale roughness.

Similarly, using the small-perturbation theory, we calculated Bragg-type scattering on the small-scale roughness for HH-polarization. In Figure 4, the HH-polarization signal of Bragg-scattering origin is compared with the signal from the breaking wave that does not have those Bragg-scattering ripples. One can see that for this case of a strongly nonlinear breaking wave, scattering for a breaking wave at HH-polarization exceeds the level of Bragg scattering during the final stage of wave breaking.
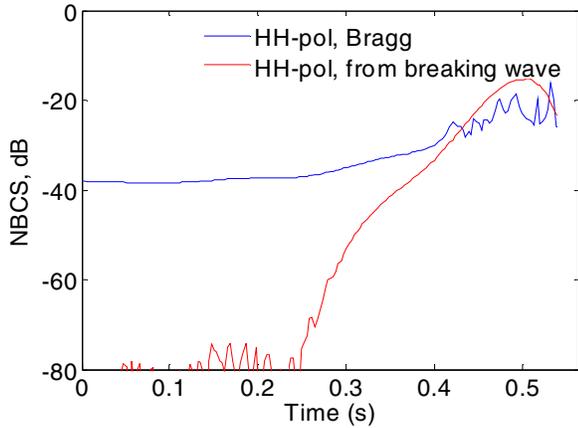
Figure 4. HH-polarization NBCS at 68.5° incidence for a nonlinear breaking wave and for small-scale roughness.

In Figure 5, we combined the cross sections caused by steep breaking waves and by Bragg scattering. This plot demonstrates that the total signal at HH-polarization finally exceeds the total signal at VV-polarization. This is an example of sea spike with HH > VV that resembles the one observed in sea radar clutter at low grazing angles.
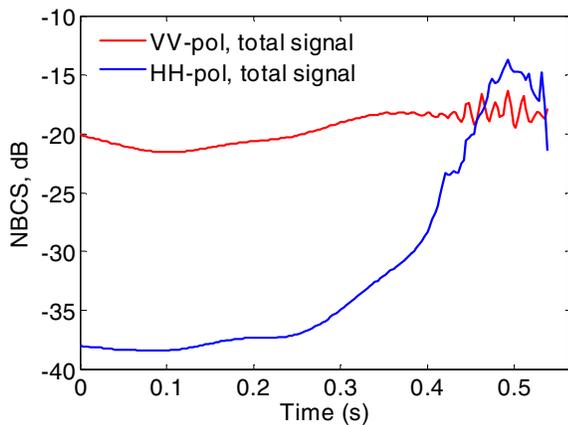
Figure 5. Comparisons between total NBCS on two polarizations at 68.5° incidence for a breaking wave with small-scale roughness on it.

The most radical, spike-like increase, as expected, occurs when HH-polarization dominates VV-polarization during the last 0.1 seconds, when the wave is passing through the cresting and involution stages. The onset of jetting leads to a relative decrease of backscatter, with HH-polarization becoming smaller than VV-polarization

Figure 6 shows Doppler spectra at two polarizations calculated over the last 0.154 s, when the sea spike took place. One can see pronounced peaks at positive frequencies due the upwind orientation, with HH-polarization dominating VV-polarization.

In conclusion, the simulated NBSC and Doppler spectra correspond well to the known features of radar scattering from ocean breaking waves [1, 2].
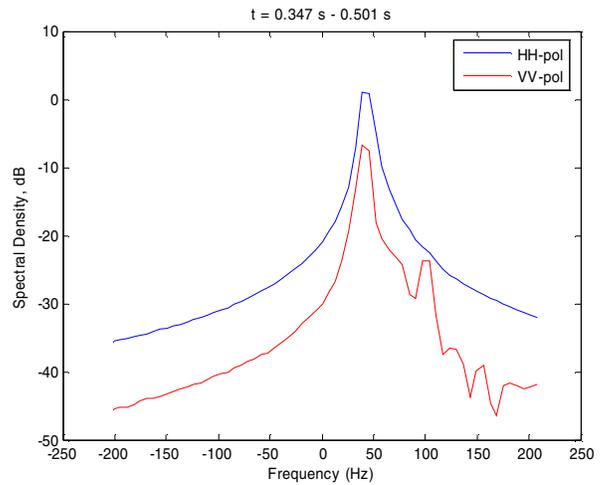
Figure 6. Doppler spectra of the sea spike for HH- and VV-polarization at 68.5° incidence and in an upwind direction.

REFERENCES

[1] A.T. Jessup, W.C. Keller, and W.K. Melville, "Measurements of sea spikes in microwave backscatter at moderate incidence," *J. Geophys. Res.*, vol. 95, pp. 9679–9688, 1990.

[2] Y. Liu, S.J. Frasier, and R.E. Mcintosh, "Measurement and classification of low-grazing-angle radar sea spikes," *IEEE Trans. Antennas Propagat.*, vol. 46, pp. 27–40, 1998.

[3] A.G. Voronovich and V.U. Zavorotny, "Theoretical model for scattering of radar signals in K_u- and C-bands from a rough sea surface with breaking waves," *Waves Random Media*, v. 11, pp. 247–269, 2001.

[4] J.C. West, J.M. Sturm, and S.-J. Ja, "Low-grazing scattering from breaking water waves using an impedance boundary MM/GTD approach," *IEEE Trans. Antennas Propagat.*, v. 46, pp. 93–100, 1998.

[5] D. Holliday, L.L. DeRaad, Jr., and G. J. St.- Cyr, "Sea-spike backscatter from a steepening wave," *IEEE Trans. Antennas Propagat.*, v. 46, pp. 108–113, 1998.

[6] A.G. Voronovich and V.U. Zavorotny, Scattering of electromagnetic waves from breaking surface gravity waves, *Proc. Int. Conf. Electromagnetics in Advanced Applications (ICEAA'05)*, Torino, Italy, 2005.

[7] A.G. Voronovich and V.U. Zavorotny, "The effect of steep sea-waves on polarization ratio at low grazing angles," *IEEE Trans. Geosci. Remote Sensing*, v. 38, pp. 366–373, 2000.